Precoding for TDD and FDD in Measured Massive MIMO Channels

Nielsen, Jesper Ødum; Karstensen, Anders; Eggers, Patrick Claus Friedrich; De Carvalho, Elisabeth; Steinböck, Gerhard; Alm, Martin

Published in:
IEEE Access

DOI (link to publication from Publisher):
10.1109/ACCESS.2020.3033166

Publication date:
2020

Document Version
Publisher's PDF, also known as Version of record

IEEE Access
Multidisciplinary | Rapid Review | Open Access Journal

Received September 21, 2020, accepted October 5, 2020, date of publication October 22, 2020, date of current version November 4, 2020.

Digital Object Identifier 10.1109/ACCESS.2020.3033166

Precoding for TDD and FDD in Measured Massive MIMO Channels

JESPER ØDUM NIELSEN[1], ANDERS KARSTENSEN[1], PATRICK C. F. EGGERS[1], (Member, IEEE), ELISABETH DE CARVALHO[1], (Senior Member, IEEE), GERHARD STEINBÖCK[2], AND MARTIN ALM[2]

[1]Department of Electronic Systems, Technical Faculty of IT and Design, Aalborg University, 9220 Aalborg, Denmark
[2]Huawei Technologies Sweden AB, 41250 Gothenburg, Sweden

Corresponding author: Jesper Ødum Nielsen (jni@es.aau.dk)

This work was supported by Huawei Technologies Sweden AB, Gothenburg, Sweden.

ABSTRACT This paper analyzes the performance of well-known precoding schemes for massive multiple-input multiple-output (MMIMO) systems. The investigations are based on extensive measurements made with a sounding system capable of capturing the dynamic channels towards users moving in many different outdoor scenarios. Assuming ideal channel state information (CSI), results show that the mean sum-rate of the maximum ratio transmission (MRT) precoder varies considerably with the scenario, *e.g.*, from 6.5 to 14.5 bit/s/Hz (10%- and 90%-percentiles) for a 64 element uniform linear array (ULA) at the base station (BS), while the zero-forcing (ZF) and signal to leakage and noise ratio (SLNR) precoders are more robust and higher performing with variation from 13.4 to 16.3 bit/s/Hz in the same conditions. However, when the CSI is non-ideal the performance drops. With the CSI delayed corresponding to movement of about 1/5 of a wavelength, the ZF and SLNR mean sum-rate is 60–92% of that achieved with ideal CSI (10%- and 90%-percentiles). More statistics for different massive array sizes with both delay and frequency offset CSI are given in the paper.

INDEX TERMS Cellular communications, channel sounding, massive MIMO, multi-user, precoding, radio propagation measurements, sum-rate, time-varying channel.

I. INTRODUCTION

In the last few years the MMIMO technology has emerged as candidate for 5G wireless communication systems [1]. One of the main benefits of MMIMO is the possibility of increased system capacity obtained mainly by added complexity on the infrastructure side [2], [3]. The number of antenna elements on a MMIMO BS is counted in several tens or even hundreds, much larger than today's up to eight elements in long-term evolution (LTE) systems.

In MMIMO systems, simultaneous transmission to different users in the same time/frequency resource is possible via precoding that generally depends on the radio channel from the BS towards all the users. For a large number of antennas the channels towards different users become orthogonal, assuming sufficient scattering in the channel. In those conditions, relatively simple precoding schemes are nearly optimal [4]. An additional benefit of the many antennas are more stable channels, when the so-called channel hardening occurs.

The associate editor coordinating the review of this manuscript and approving it for publication was Cunhua Pan.

Since the channel generally is dispersive and changing due to movement of the users and other objects in the environment, the CSI is both time and frequency dependent and must be estimated regularly. This is typically done using training symbols embedded in the traffic data and thus with an associated trade-off between the CSI accuracy and the amount of training data.

In a time-division duplex (TDD) system the precoding in the down-link (DL) is based on CSI estimated by the BS utilizing training symbols sent by the mobile stations (MSs) and assuming reciprocity of the channel. If the system is not designed carefully, the resulting CSI may be inaccurate, *e.g.*, in high speed scenarios, leading to degraded precoder performance. For a frequency-division duplex (FDD) system the up-link (UL) and DL channels are separated by the duplex distance which again may lead to degraded performance, if the CSI estimates are based on training symbols on the UL channel and time dispersion causes frequency decorrelation between UL and DL bands. Alternatively, the estimation is based on training symbols sent on the DL and then transferred to the BS from each MS. However, with many users this could be a time- and data-consuming procedure that may

lead to inaccurate CSI. While MMIMO may seem best suited for TDD operation, spectrum allocation is often available in paired duplex bands and FDD may nevertheless need to be considered. The work in [5] compares performance of TDD and FDD systems in measured channels, assuming perfect CSI knowledge. A large degradation was found for FDD compared to TDD systems in many channels, unless they are in line of sight (LOS) conditions and have high Ricean factors.

Accurate evaluation of MMIMO systems needs to be carried out using real channels, since MMIMO may exploit channel features that are not included in current channel models. Several testbeds have been implemented such as the TDD system described in [6] operating at 2.6 GHz, or the TDD system at 3.5 GHz described in, *e.g.*, [7]–[9]. Another example of a TDD testbed is used in these works [10], [11]. Generally, the testbeds include most of the core functionality of several MSs and one or more BSs, including real-time signal processing, in order to verify performance in realistic conditions. These systems are highly complex involving many necessary implementation and design choices, and typically the works focus on the throughput of particular implementations and its dependency on, *e.g.*, the type of environment, the number of users or the distances between them.

Another overall group of existing works focus on the fundamental mechanisms of MMIMO using channel sounding data. The main challenge in measuring MMIMO channels lies in acquiring data from all channels corresponding to the combinations of all BS antenna element ports to all the MS antenna ports. For complexity and cost reasons the high number of channels may be obtained by moving a single antenna, or a small array, to different physical locations, thereby creating a virtual array which is considered a MMIMO array in analysis. A virtual array measurement may take a long time, even many minutes, but this can be acceptable if the channel may be considered essentially static, *e.g.*, in an indoor scenario with no activity, or outdoors at nighttime. A few example works using virtual arrays include [1], [4], [5], [12]. Testbed systems can also provide data on the MMIMO channel, thereby achieving some of the same functionality as dedicated sounders [8].

While virtual array based investigations have been used to show large capacity gains over conventional systems, realistic evaluation of issues like precoding schemes and their susceptibility to inaccurate CSI can only be carried out with joint knowledge of all channels in a dynamically changing scenario. Although testbeds handle the dynamic case, the performance of a specific testbed implementation does not necessarily reflect the full potential of the MMIMO channel.

Only a few previous works are based on simultaneous recording[1] of all the individual links of MMIMO channels to multiple users. Some of the earliest works are [13], [14], and [15], [16] are more recent examples, all investigating various aspects of MMIMO of systems, assuming ideal knowledge of CSI. The works in [17], [18] analyze the impact of aging CSI on capacity but are both limited to, respectively, one or a few scenarios.

The contributions of this paper are based on an outdoor sounding measurement campaign where the full MMIMO channel between a BS and two moving MSs is measured. The measurement system used employs fully parallel sub-arrays and fast switching for the massive array on the BS, allowing analysis of data from a dynamically changing environment. Many different scenarios are considered, both in LOS and non line of sight (NLOS), as well with varying distances between the users (see Section II). As described in Section III–IV, the analysis focuses on three well known precoding schemes, MRT, ZF and SLNR, and studies the changes in sum-rate statistics among the different scenarios. Described in Section V, the case with ideal CSI is used as reference and the degradation is observed with different amounts of CSI delay, as in a TDD system. Similarly, changes in statistics of the sum-rate are obtained for CSI with varying degree of frequency offset, as in a FDD system. Section VI concludes the paper.

II. MEASUREMENTS

The measurements used in the current work are acquired with a channel sounder operating at a center frequency of 3.5 GHz. The sounder employs 16 fully parallel Tx branches and 8 fully parallel Rx branches, and by utilizing fast 1:16 switching on each Rx branch, the system can measure all channel combinations of a 128 $\times$ 16 (Rx $\times$ Tx) MMIMO system quasi-simultaneously in about 1.31 ms. This allows studies of realistic channels of a MMIMO system, including both small- and large-scale fading as users move, as well as interference to non-intended users in a MMIMO system. The sounder has a bandwidth of about 100 MHz and is described further in [19].

Two MSs were used, both consisting of a trolley moved by a person, see Fig. 1 (left). Each MS was equipped with a circular array of eight patch elements, connected to eight of the Tx channels of the sounder, via 30 dBm power amplifiers.

The MS arrays are designed to allow analysis of directional channel properties. The elements have a measured 3 dB beamwidth of about 75° in azimuth angle and about 55° in elevation angle. The array centers were 167 cm above the ground, a compromise between a realistic height of a user device while minimizing unwanted disturbance from the trolley, equipment, and the person moving the trolley. Although arrays are used at the MSs, the channels for the eight elements at each MS are simply summed with equal weights in this work, thus approximating a single omni-directional antenna (in azimuth). The two MSs represent $K = 2$ users in the following.

The massive array is depicted in Fig. 1 (center) and consists of two rows of each 64 elements. The elements are vertically polarized Vivaldi-type horn antennas mounted at 5 cm distance, and each row forms a 3.2 m long ULA. The elements

[1] in practice, within a time much shorter than the coherence time of the channel

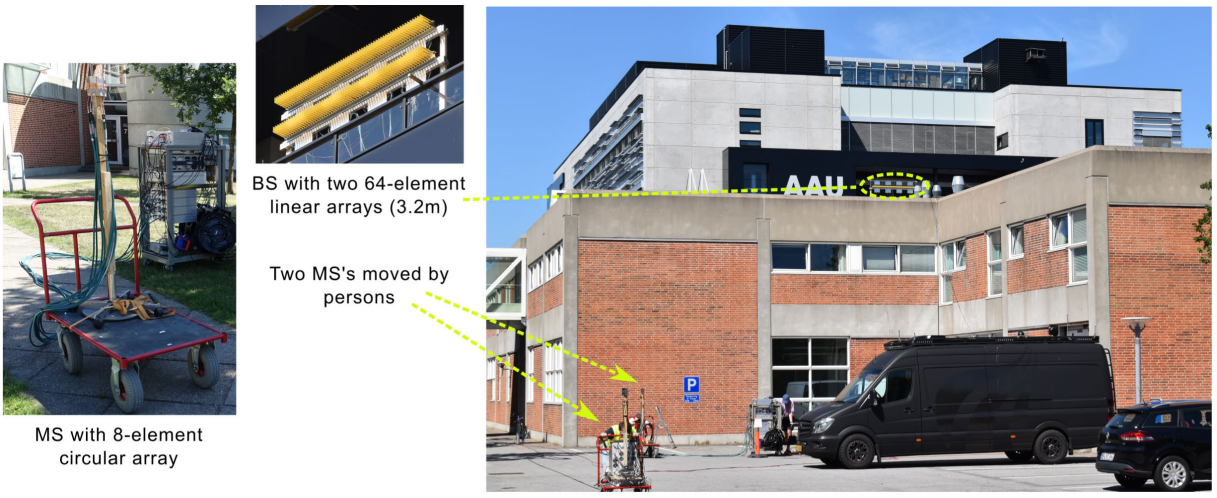

FIGURE 1. Measurements in a NLOS scenario with two MS on trolleys with circular arrays and the 128-element massive array on the 4th-floor balcony of the building in the back.

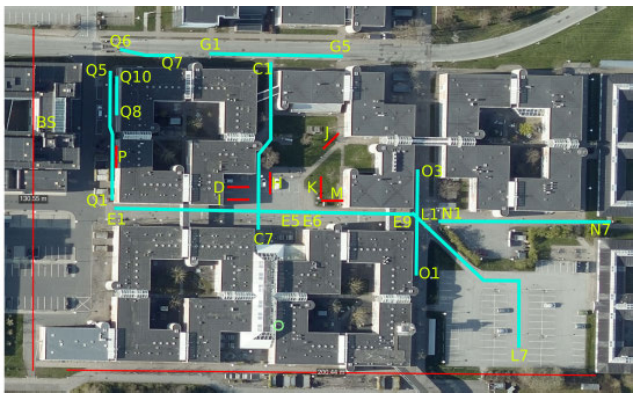

FIGURE 2. Overview map of the different measurement locations. Aerial photo from Agency for Datasupply and Efficiency, April 2019 [20].

have a measured 3 dB beamwidth of about 100° and 51° in azimuth angle for a center and edge element, respectively, and about 35–37° in elevation angle. In this work only the 64 elements in the top row are used.

All the measurements were carried out on the Aalborg University campus, as shown in the overview map in Fig. 2. A number of routes are indicated on the map, each denoted by a letter. The map also indicates the location of the massive array which is mounted on the 4th floor of a building, about 16.1 m above the ground, mimicking a BS overlooking the area below. Most of the other buildings in the area in front of the massive array are two-story, except those on the far right of the map (one-story) and lower right (three-story).

All measurements are done in the same way; the two MSs are moved by two persons at slow walking speed. Each measurement lasts 15 seconds, during which snapshots of the MMIMO channel are recorded at a 60 Hz rate to achieve 900 snapshots. A specific measurement is identified by the routes the MSs follow, where a letter denotes an overall route and an integer specifies the section of that route. For example C2 denotes the 2nd section of route C. The measurements are grouped into different scenarios, each characterized by MS-A repeating the same short track, while MS-B performs several

TABLE 1. Overview of measurements.

MS-A	MS-B	Description
D	C1–C7	Different AoA. MS-A/B close at C6
I	E1–E5	Different AoA & distances. MS-A/B close at E3.
J	E6–E9	Different AoA & distances E6 in open, E7–9 near buildings.
H	G1–G5	Different AoA & distances Different clusters exp. for MS-A/B
K	L1–L7	MS-B is in a parking lot, moving away. Possible diffraction over building and possible reflection on buildings East/South of MS-B. Different clusters are expected for MS-A and MS-B.
M	N1–N7	MS-A is in courtyard, with MS-B moving away next to parking lot. Different clusters are expected for MS-A and MS-B.
K	O1–O3	MS-A is in courtyard, MS-B moving along bicycle path, crossing area between two buildings with much stronger main path. Different clusters are expected for MS-A and MS-B.
P	Q1–Q5	Both MS are on sidewalk opposite the BS building, below main array direction. MS-B is moved along sidewalk, with some bicycle sheds partly blocking LOS. MS-A/B pass at Q2.
P	Q6–Q7	MS-B is moving in the bus lane, starting from corner in LOS and moving into NLOS.
P	Q8–Q10	MS-B moving down ramp to basement.

short consecutive sections that together form one track/route. The measurements were done in very different scenarios; *e.g.*, some where the MSs are close to the BS, are widely separated in angle towards the BS or in distance, while in some cases the MSs are close to each other. An overview of all the measurements is given in Table 1. In total 50 measurements were made.

III. CHANNEL AND NORMALIZATION

The measured data are represented by impulse responses (IRs) for each combination of BS antenna element, MS antenna element and snapshot index. In order to allow simulation of channel estimation delays smaller than the snapshot measurement interval, the data is interpolated (using splines)

as a first step.[2] Thereby the snapshot rate is increased to 600 Hz, corresponding to a period of $T_s \simeq 1.7$ ms, and the number of snapshots is $R = 9000$. After introducing the estimation delay (see below), decimation is performed so that the rate is again 60 Hz.

Following a Fourier transform, $g_k(l, r) \in \mathbb{C}^{M\times 1}$ denotes the channel coefficients for the M BS array elements for the kth user, the rth snapshot index and for frequency sub-channel l. The sub-channels are separated by about 0.67 MHz. From this data sub-channels are selected and used as the actual (target) channel and the estimated channel, respectively,

$$h'_k(r) = g_k(l_{\text{actual}}, r + r_0) \tag{1}$$
$$\tilde{h}'_k(r) = g_k(l_{\text{estim}}, r) \tag{2}$$

with $r \in \{1, 2, \ldots, R - r_0\}$ where l_{actual} is the sub-channel index used for the actual broadcast channel and l_{estim} is the sub-channel index used for the estimate of that channel, thus allowing investigation of different duplex distances in FDD systems as well as TDD systems where $l_{\text{estim}} = l_{\text{actual}}$. The time delay in obtaining the channel estimate is emulated using an integer $r_0 \geq 0$ times the snapshot time difference T_s. Note that although different sub-channels are used for FDD, all the investigated systems are utilizing the same frequency, in case of TDD, or set of frequencies in case of FDD, as no scheduling is considered.

Before analysis the channels are normalized to the average power over snapshots and elements, preserving any differences between the elements of the array as well as among the users,

$$h_k(r) = \frac{h'_k(r)\sqrt{MK(R - r_0)}}{\sqrt{\sum_{r=1}^{R-r_0}\sum_{k'=1}^{K}\left\|h'_{k'}(r)\right\|^2}} \tag{3}$$

where $\|\cdot\|$ denotes the Euclidean norm. Similarly, the normalized estimated channel $\tilde{h}_k(r)$ is obtained from $\tilde{h}'_k(r)$. In the following $H(r) \in \mathbb{C}^{M\times K}$ denotes the matrix with columns given by $h_k(r)$ for each of the K users. Likewise, $\tilde{H}(r)$ is the corresponding matrix of estimated channels.

IV. PRECODING

Generally the precoding done at the BS introduces weighting of the array element outputs used to transmit the vector $x(r) \in \mathbb{C}^{K\times 1}$ of symbols to be conveyed to the K users. Denoting the weight matrix by $W^n(r) \in \mathbb{C}^{M\times K}$ the received signal $y(r) \in \mathbb{C}^{K\times 1}$ at the users can be modeled as

$$y(r) = H(r)^{\dagger} W^n(r)\Gamma(r)x(r) + v(r) \tag{4}$$

where $()^{\dagger}$ denotes the conjugate transpose operator. The weight matrix is composed of the vectors associated with each user k

$$W^n(r) = \left[w_1^n(r) \cdots w_K^n(r)\right] \tag{5}$$

where each column vector is normalized so that the mth element of the vector for the kth user is $w^n_{k,m}(r) = w_{k,m}(r)/\|w_k(r)\|$. The matrix $\Gamma(r) = \text{diag}[\gamma_1(r), \ldots, \gamma_K(r)]$ in (4) determines the power distribution and $v(r)$ is the channel noise.

Finding the optimum weights and power allocations is difficult, but fortunately promising sub-optimum solutions exist [21]. The different types of weighting used in this work are described briefly below; further details may be found in [22]. All the selected schemes are sub-optimal and linear, chosen for their relatively low complexity. A recent example of a more advanced precoding scheme is given in [23], based on hybrid analog/digital beamforming. Though it is not considered in the current work, it may be a possiblity if a better performance can justify its higher complexity. A single-cell scenario is assumed and the noise level is identical for all receivers.

A. MAXIMUM RATIO TRANSMISSION (MRT)

Similar to a matched filter, the weights used in the MRT precoder are given by

$$W_{\text{MRT}}(r) = H(r) \tag{6}$$

Interference may occur between users, unless the channels are highly orthogonal. For a low signal to noise ratio (SNR) scenario the MRT may be beneficial, since the effects of interference are dominated by that of noise.

B. ZERO-FORCING (ZF)

If $M > K$ the inter-user interference may be eliminated by using the ZF weights

$$W_{\text{ZF}}(r) = H(r)\left[H^{\dagger}(r)H(r)\right]^{-1} \tag{7}$$

which is beneficial for non-orthogonal users and in high SNR situations. For low SNRs the ZF precoder is outperformed by the MRT precoder [21].

C. MAXIMUM SIGNAL TO LEAKAGE AND NOISE RATIO (SLNR)

This precoder defined in [22] maximizes the SLNR, *i.e.*, the ratio of the desired signal power for a user to the noise plus interference caused at the other users. This precoder is given by

$$W_{\text{SLNR}}(r) = H(r)\left[I_K/\eta + H^{\dagger}(r)H(r)\right]^{-1} \tag{8}$$

where I_K is the identity matrix and η is the SNR. The SLNR approach is similar to the *regularized inverse* or regularized zero-forcing (RZF), where the factor for the identity matrix may differ in various implementations, as may the associated power allocation [22], [24], [25]. In addition to the CSI, also the SNRs at the receivers need to be known or estimated.

D. CLASSICAL BEAMFORMING (CBF)

While not used for precoding in this work, classical beamforming (CBF) weights are also included for analysis purposes, given by

$$W_{\text{CBF}}(r) = A(\theta) \tag{9}$$

[2] The 60 Hz IR measurement rate provides above Nyquist rate sampling for the used MS speeds, hence up-sampling makes sense.

where $A(\theta)$ is the complex vector of array element gains in the direction θ. By computing the weights and associated MS antenna output for $\theta \in \{-50°, 49°, \ldots, 50°\}$ an angular power spectrum is obtained for each channel snapshot. The element radiation patterns were obtained from anechoic room measurements of the array modules, and a Hamming window was applied.

E. POWER ALLOCATION

Following the computation of the weight matrix the users are allocated power, described in terms of γ_k^2. For mobile channels where the mean power for different users are often non-equal, the system performance may depend highly on the power allocation scheme. Finding optimum solutions is generally a complex problem depending on the channel, see [26] and references therein. In the current work the water filling procedure is followed, which is optimum for the ZF weights but sub-optimum for MRT and SLNR [22]. Using water filling, the available Tx power is distributed according to the instantaneous channel conditions with the code provided by Björnson *et al.* [27]. Once both the weight matrix and power allocation have been determined, the resulting signal to interference plus noise ratio (SINR) for the kth user is computed as

$$\chi_k(r) = \frac{\rho_{k,k}^2(r)}{\sigma_v^2 + \sum_{\substack{l=1 \\ l \neq k}}^{K} \rho_{k,l}^2(r)} \tag{10}$$

where σ_v^2 is the assumed noise power and

$$\rho_{k,l}^2(r) = \left| \gamma_l(r) \sum_{m=1}^{M} h_{k,m}^*(r) w_{l,m}^n(r) \right|^2 \tag{11}$$

where $h_{k,m}(r)$ is the mth element of the vector $h_k(r)$. Note that the $h_{k,m}(r)$ values are that of the actual channel, as opposed to the estimated channel used in determining W^n and Γ. Finally, the sum-rate is given by $R(r) = \sum_{k=1}^{K} \log_2 [1 + \chi_k(r)]$.

V. RESULTS

This section presents performance results obtained with the different precoders described above, based on the measurements with two users, as described in Section II. It is noted that while the two-user scenario is not where MMIMO would typically be employed, it does allow investigations of precoder performance sensitivity to inaccurate CSI.

A. PERFORMANCE WITH IDEAL CSI

As an ideal reference case, the results discussed in this section are presuming that ideal knowledge of the CSI is available at the BS, so that there is no estimation delay and the same frequency channel is used, *i.e.*, $r_0 = 0$ and $l_{\text{actual}} = l_{\text{estim}}$ in (1-2).

Fig. 3 shows some example results obtained with measured data from a specific measurement route. The two plots at the top shows, respectively, the CBF spectrum for the channel towards the two users, as they move. The plot at the bottom of Fig. 3 shows the sum-rates obtained for each snapshot using the three different precoders and an SNR of 10 dB.

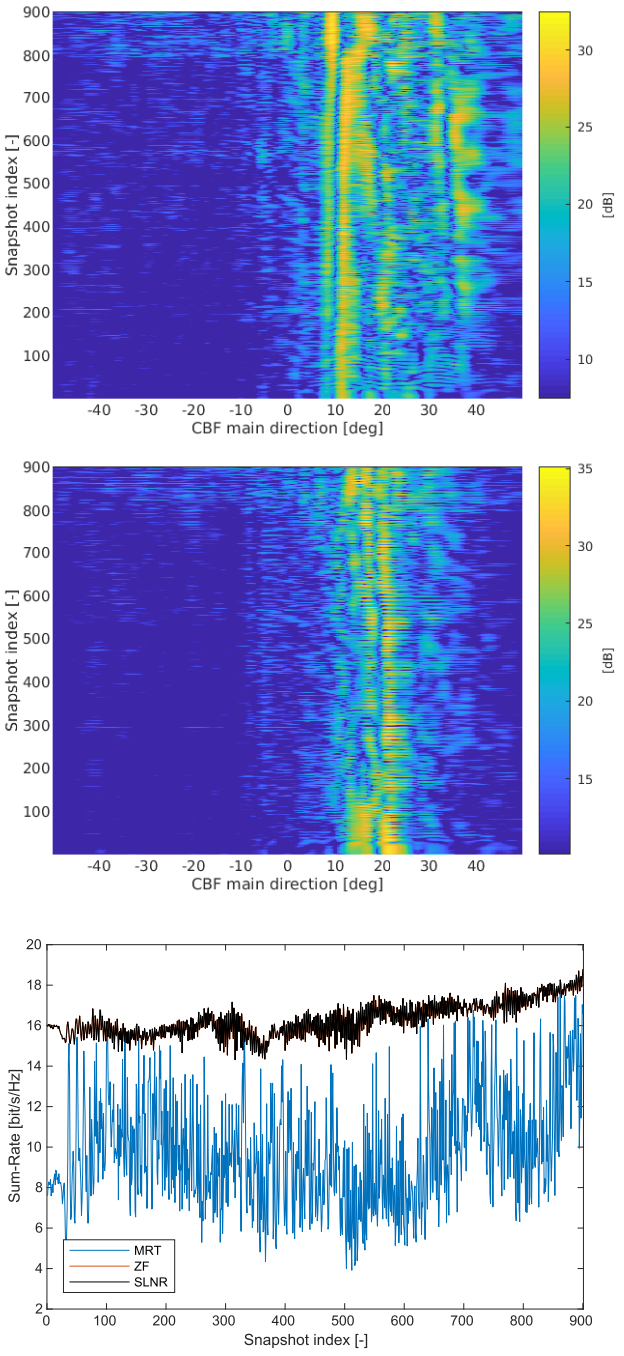

FIGURE 3. Classical beamforming spectrum for user one (top) and user two (middle). Corresponding sum-rates for MRT, ZF, and SLNR precoders (bottom plot), for ideal CSI, an SNR of 10 dB, and $M = 64$ array elements. The results are for the I/E6 measurement scenario. Note, the curves for ZF and SLNR are nearly identical.

In this scenario the main directions to the two users are overlapping to a large degree. As expected in this scenario, the ZF and SLNR precoders are superior to MRT both in terms of a generally higher sum-rate as well as lower sum-rate variation caused by the random channel.

A comparison of results from the measured data with similar results achieved in a simulated Gaussian independent and identically distributed (IID) channel is given in Fig. 4.

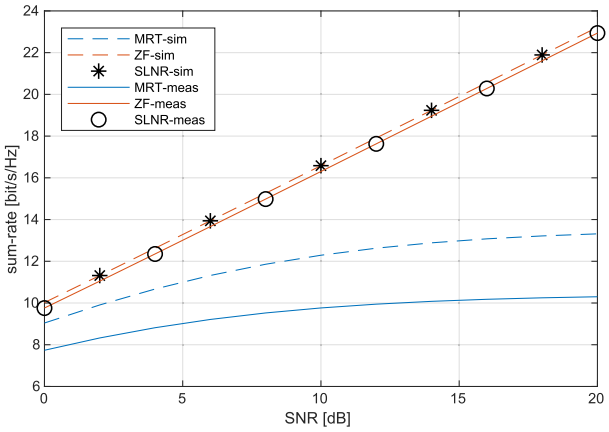

FIGURE 4. The mean sum-rate achieved for the MRT, ZF, and SLNR precoders with $M = 64$ in both a measured channel (I/E6 scenario) and a simulated Gaussian channel.

The MRT precoding performs much better in the simulated channel than in the measured channel, since the precoder benefits from the uniform gain distribution versus angle in the model channel, as opposed to the clustering in the measured channel that leads to increased interference between the users (see top plots in Fig. 3). For other measurements where the users are more separated in angle, the mean sum-rate can be much higher for the measured channel than for the Gaussian channel. The ZF and SLNR precoders yields close to the same results when more than about 8 antenna elements are used on the base.

As exemplified above, the achieved sum-rate depends on the channel as well as the precoder, number of antennas, and the SNR. An overview of the variations is given in Fig. 5 in terms of percentiles of the instantaneous sum-rates for a specific measurement, assuming different conditions. For the SLNR precoder the median sum-rate increases close to linearly with the SNR for $M \geq 8$ (also for ZF, not shown), which is not the case for MRT that levels off. Also, the 10% to 90% interval gets smaller with increasing M for SLNR while it is increasing for MRT.

The sum-rate is determined by the SINR. For ZF and SLNR the interference term is zero or small and hence the performance is mainly determined by the power of the desired signal. This gets more and more stable with increasing array size, since random variations due to the multipath gets averaged out. For MRT both the desired and interfering signals are present, but while the desired signal stabilizes with array size, the interference term fluctuates due to the changing channel of the interfering user. Hence, depending on the channel, the interference terms may both increase or decrease with array size.

Not only does the performance depend on the number of array elements, the SNR, and the type of precoder, the characteristics of the channel may also have a significant influence. Fig. 6 shows the variation in the mean sum-rate obtained for each of the different measurement locations. The mean is computed over all the snapshots in each measurement. Clearly, there is a large variation in the mean sum-rate,

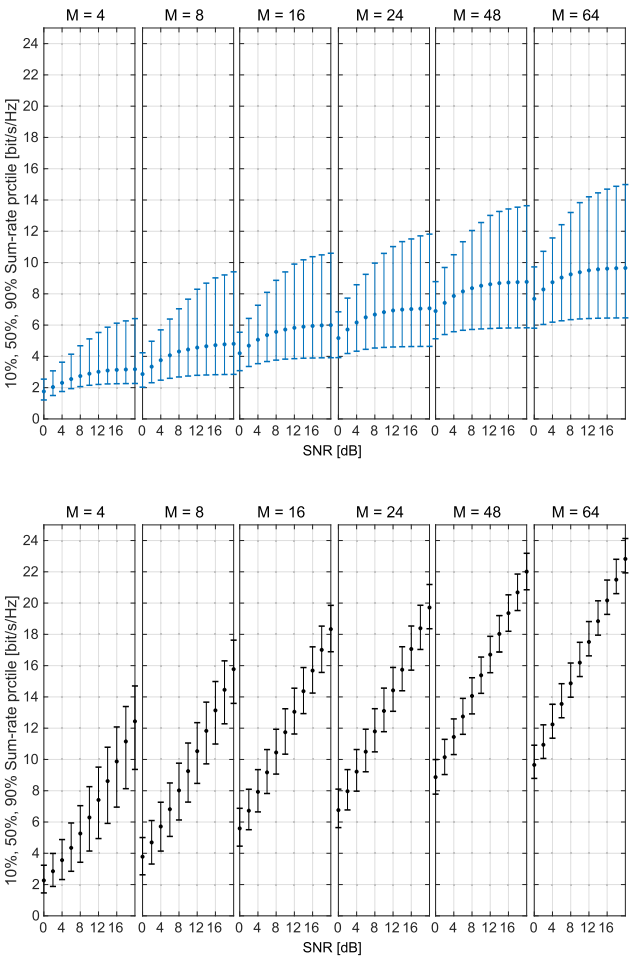

FIGURE 5. 10%-, 50%-, and 90%-percentile of the sum-rate shown as vertical lines for different SNR values (x-axis) and number of elements M in the BS array (sub-plots). Results for the MRT precoder (top plots) and for the SLNR precoder (bottom plots). All results are for the I/E6 measurement scenario.

depending on the measurement location. An overview of the results is given in Fig. 7, where 10%-, 50%-, 90%-percentiles indicates the variation in the mean sum-rate obtained for all the measurements, assuming different array sizes (sub-plots), the three types of precoders and an SNR of 10 dB. As expected, the MRT precoder has a smaller median value and larger variation in the mean sum-rate, compared to the ZF and the SLNR precoders. This is true for all array sizes, but the difference increases with M. The ZF and SLNR precoders are less sensitive to the propagation environment than the MRT precoder, as evidenced by the shorter vertical lines. Further, the sensitivity gets smaller with an increasing number of antenna elements. Hence, the extra degrees of freedom are effective in obtaining the same sum-rate performance irrespective of a highly changing propagation environment.

B. PERFORMANCE WITH DELAYED CHANNEL INFORMATION

The results discussed in this section focus on the precoder performance when the CSI arrives with a delay. This may happen in a TDD system due to the duplex switching time,

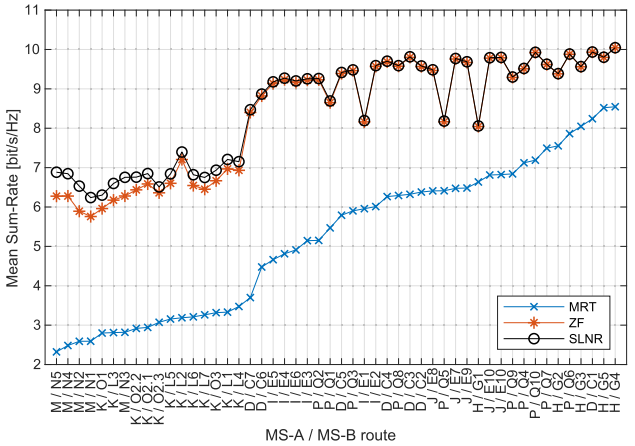

FIGURE 6. Sum-rate averaged over the measurement route, shown versus the route followed by MS-A/B and sorted for increasing MRT precoding results. The assumed number of BS elements is $M = 8$ and the SNR is 10 dB.

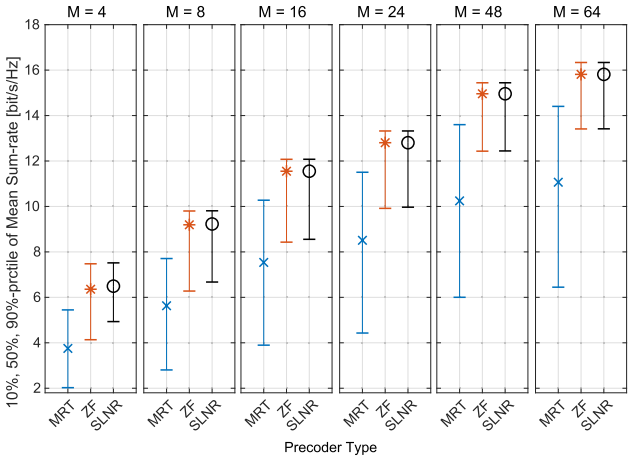

FIGURE 7. The variation in the mean sum-rate depending on the measurement scenario and array size. Each vertical line indicate 10%-, 50%- and 90%-percentiles among all measured scenarios. An SNR of 10 dB is used.

or in a FDD system where the CSI is based on UL transmissions from each mobile. The computation of the precoder performances are done the same way as in the previous section, except that the CSI used to compute the precoder weights and the power allocations is more or less obsolete with respect to the channel on which the precoder is applied.

As described in Section III, the channel estimation delay applied is $r_0 T_s$, where $r_0 \in \{0, 1, \ldots 10\}$ and $T_s \simeq 1.7$ ms. Assuming a 1 m/s speed of the MS, the delay range studied corresponds to distance of about $1/50$ up to about $1/5$ of a wavelength.

The assumed delays may also be related to 5G NR, where the radio link for each sub-channel is time-multiplexed, and different MSs are scheduled into 1 ms sub-frames in which both UL and DL transmission may happen [28]. To compute precoding vectors and power levels, the BS must estimate the UL channel from all MSs, thus resulting in delays of several ms in obtaining the full MMIMO channel, where each MS adds minimum 1 ms delay.

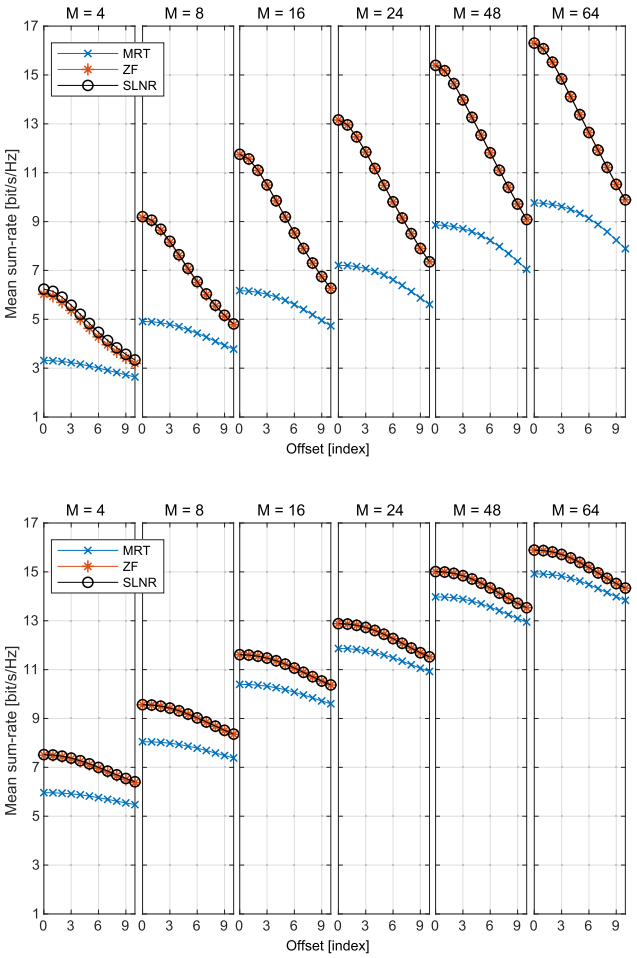

FIGURE 8. The mean sum-rate for the MRT, ZF, and SLNR precoders for different combinations of BS array size M and the channel estimation delay (integer times 1.7 ms). The SNR is 10 dB for the well separated H/G3 scenario (bottom) and the overlapping I/E6 scenario (top).

In order to limit the analysis, only the mean sum-rate will be analyzed in the following, although the distribution of the sum-rate, due to the changing instantaneous channel, may also depend on the estimation delay. Some examples of the mean sum-rates obtained for a specific measurement are shown in Fig. 8, where each sub-plot shows the mean sum-rate as function of the delay index. Clearly, there is generally a large degradation in the mean sum-rate, *e.g.*, from about 16.3 to 9.9 bit/s/Hz when the delay in increased from $r_0 = 0$ to $r_0 = 10$ for $M = 64$ and the SLNR precoder.

A general tendency in the results is that for measurement scenarios where the main paths to the two users are well separated in angle, the degradation due to the estimation delay is smaller than when users are not well separated. In other words, accurate CSI is most critical when the zero-forcing abilities of the ZF and SLNR precoders are really needed to avoid inter-user interference. For example, the bottom plots of Fig. 8 are for a well separated case, with small degradation and where also the MRT precoder shows good performance, compared to the case in the top plots, where the main paths to users are more interleaved.

Noting the dependence on the environment, statistics were derived of the degradation in the mean sum-rate obtained in

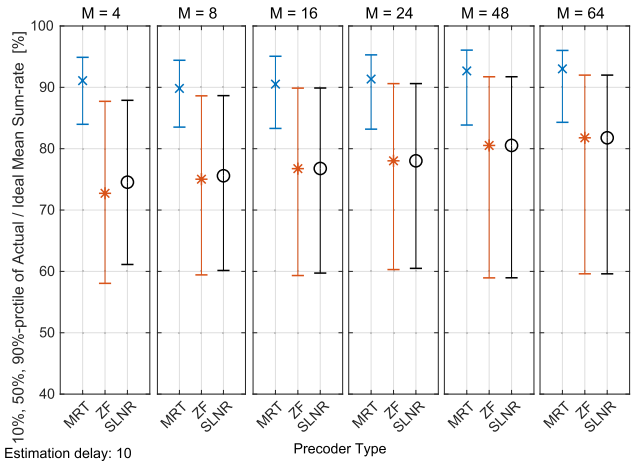

FIGURE 9. **Mean sum-rate obtained with delayed CSI as ratio to mean sum-rate obtained with ideal CSI (in %). The plot shows 10%-, 50%, 90%-percentiles of results for different measurement scenarios.**

different environments. For brevity, the degradation observed with a single estimation delay of $r_0 = 10$ was considered, using the ratio

$$\xi_{\text{delay}} = 100 \cdot \frac{\mu_{\text{del}}(10)}{\mu_{\text{del}}(0)} \tag{12}$$

i.e., the mean sum-rate achieved with a delay of 10 as a percentage of the mean sum-rate achieved with no delay. In the formula $\mu_{\text{del}}(r_0)$ is the mean sum-rate computed over the measurement snapshots assuming an estimation delay of r_0. The above ξ_{delay} was computed for all the measured scenarios, which values were then used for computing percentiles. Fig. 9 shows results for different choices of array size and precoder type. In each case the 10%-, 50%-, 90%-percentiles are shown as the lower, middle, and top point of the line, respectively. As before, the ZF and SLNR performances are nearly identical.

Median rates of about 73% were found for a small $M = 4$ array increasing up to about 82% for an $M = 64$ array. The MRT precoder is generally more robust towards the estimation delay, with median rates of about 90% or above for all array sizes. Also, the variation among the different scenarios, as indicated by the 10%- to 90%-percentile interval, is much higher for the ZF and SLNR than for the MRT precoder. The ability of the SLNR and ZF precoders to maintain a high sum-rate irrespective of the scenario, at least when using a large array as described in Section V-A, is highly dependent on accurate CSI. The figure shows that with delayed CSI the mean sum-rate depends highly on the environment, so that 80% of the scenarios can only be described in a fairly large range, about 60–90% of the mean sum-rate obtained with ideal CSI.

C. PERFORMANCE WITH FREQUENCY OFFSET CHANNEL INFORMATION

The results presented in this section are for the case where the CSI is estimated using data obtained at a different frequency than that of the target channel where the CSI is applied, such as in a FDD system where UL training data is used.

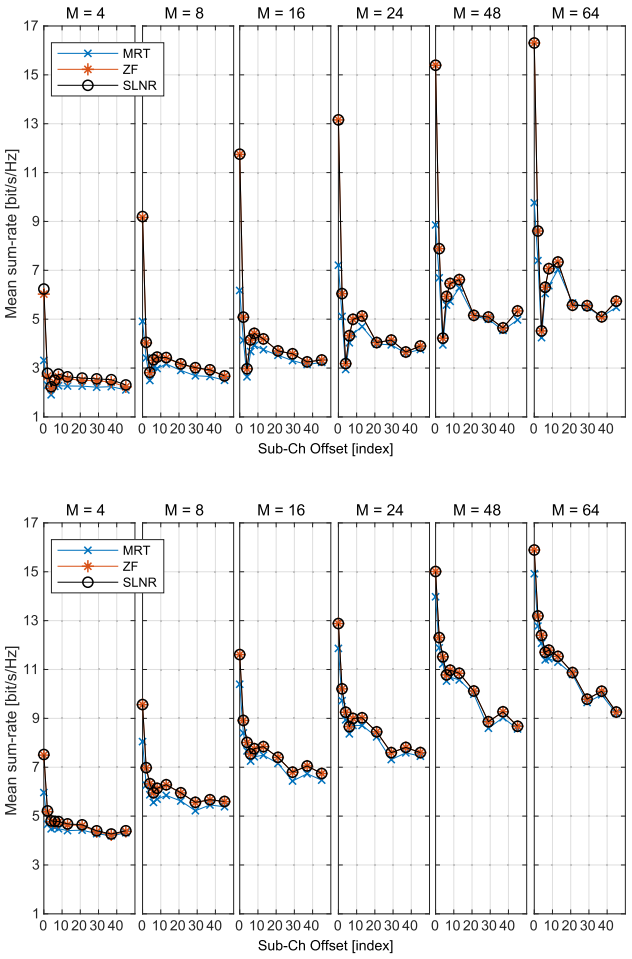

FIGURE 10. **The mean sum-rate achieved for the MRT, ZF, and SLNR precoders for different combinations of array size M on the BS and the frequency offset for the estimated channel (integer times 0.67 MHz). The SNR is 10 dB for the well separated H/G3 scenario (bottom) and the overlapping I/E6 scenario (top).**

Referring to the description in Section III, the target sub-channel is fixed by $l_{\text{actual}} = 1$ while different separations of the target and estimated sub-channel are tested by using l_{estim} in the range 1–45, *i.e.*, up to about 30 MHz separation. A time-delay $r_0 = 0$ is assumed. Note that this is not what is commonly understood by a MMIMO FDD system, where instead channel sounding is done on the DL channel followed by feedback from the MSs to the BS on the UL channel [5].

Fig. 10 shows mean sum-rates for two example measurements, where the bottom plots are for a scenario where the two users are well separated, and the top plots are for a scenario where the main cluster directions are close for the users. Each sub-plot shows the mean sum-rate versus the frequency offset between the estimated and target channel. As before, the sub-plots are for different array sizes. In all cases the mean sum-rate decreases rapidly with the offset, especially for the scenario with overlapping clusters, where for example the SLNR precoder with $M = 64$ drops from about 16.3 bit/s/Hz for no offset down to about 8.6 bit/s/Hz for a 1.3 MHz offset. Similar to what happens when estimation delay is introduced (Fig. 8), the reduction in mean sum-rate

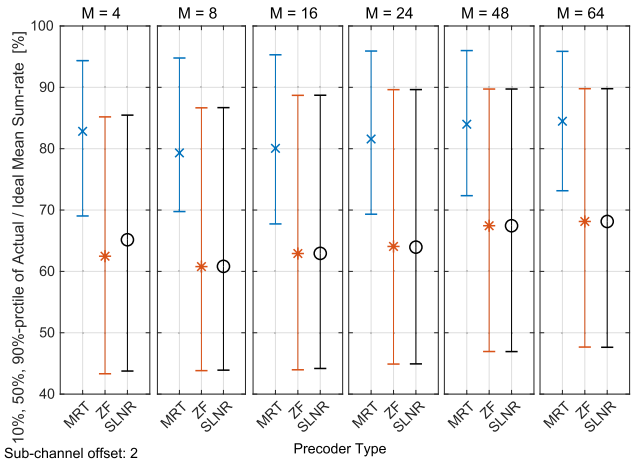

FIGURE 11. Mean sum-rate obtained with frequency offset CSI as ratio to mean sum-rate obtained with ideal CSI (in %). The plot shows 10%-, 50%, 90%-percentiles of results for different measurement scenarios.

is less dramatic, but still significant, in the well-separated scenario.

The channels for the two users have a coherence bandwidth of 1.0–1.9 MHz (0.9 level) in the two scenarios which, compared to the sub-channel bandwidth of 0.67 MHz, agrees with the rapid degradation versus offset.

The ZF/SLNR precoders are most sensitive to inaccurate CSI since the zero-forcing becomes imperfect at the same time as the gains towards the desired users are reduced. With more users, one can expect the degradation becomes more pronounced. The desired user power may also be reduced for MRT and a smaller degradation is generally seen, likely because interfering terms are present whether or not the CSI is accurate.

With the purpose of deriving statistics of the degradation in different scenarios, the following metric was used

$$\xi_{\text{freq}} = 100 \cdot \frac{\mu_{\text{ch}}(2)}{\mu_{\text{ch}}(0)} \tag{13}$$

i.e., the mean sum-rate obtained with a sub-channel offset of 2 as a percentage of the mean sum-rate obtained with no offset. In (13) $\mu_{\text{ch}}(p)$ is the mean sum-rate computed over the measurement snapshots assuming a sub-channel offset of $p = l_{\text{estim}} - l_{\text{actual}}$, and with $p = 2$ corresponding to about 1.3 MHz. Using this metric from different scenarios, percentiles were estimated, similar to the analysis of delay offsets in Section V-B. Fig. 11 shows the percentiles.

Overall, the MRT precoder degrades less than the other two precoders, with median values of 79–84% compared to values of 61–68% for the ZF and SLNR precoders. The latter two precoders are also more susceptible to scenario changes, with 80 % of the ξ_{freq} values within the range of about 45%–90%, where the MRT precoder has a more narrow range of about 68–96%. Thus, much of the performance advantage that the ZF/SLNR precoders have over the MRT is lost. Note that the statistics are derived for a frequency offset of about 1.3 MHz, much smaller than typical duplex separations where performance will be degraded even more, as in the examples of Fig. 10.

VI. CONCLUSION

The focus of this work is the performance of MMIMO systems when using imperfect CSI, considered in terms of sum-rate and assuming different precoders and number of antenna elements. The investigations are based on measurements at 3.5 GHz in 50 different outdoor scenarios, with a mixture of LOS, NLOS, and various distances between the users. In each scenario the full MMIMO channel is sampled at 60 Hz, allowing realistic analysis of the performance when the two users move around. While the case of only two users is not where a MMIMO system has its main advantage, the measured channels are useful for investigations towards the system's ability to separate the users given different assumptions.

The reference case is assuming perfect CSI. Using a MRT precoder the results are highly dependent on the scenario, in particular the separation of the users, so that the mean sum-rate varies from about 6.5 to 14.4 bit/s/Hz (range of 10%- and 90%-percentile among scenarios) for 64 array elements. This is expected, as the MRT does not attempt to avoid inter-user interference. For the same array size, the ZF and SLNR precoders both achieve mean sum-rates of about 13.4 to 16.3 bit/s/Hz. Thus, in addition to a generally higher sum-rate, a smaller variation among the scenarios is observed, due to the interference avoidance capabilities. The observed performance variations among different scenarios are not reproduced in a simple Gaussian channel model.

When a delayed, but otherwise perfect CSI is used, the superior performance of ZF and SLNR is reduced, especially in scenarios where the users are not well separated. The mean sum-rate is reduced to about 60–92% (range of 10%- to 90%-percentile among scenarios) of the performance with ideal CSI and 64 elements. The MRT precoder is affected less and reduced to about 84–96%. The results are given for a delay of 17 ms, corresponding to about 1/5 of the wavelength at slow walking speed. Results for different delays are available.

Using an excess of array elements on the BS compared to the number of users is not very effective to reduce sensitivity; the median over scenarios grows from about 75% to 82% of the corresponding sum-rate for ideal CSI when increasing the number of elements from 8 to 64.

For a FDD system one might consider obtaining the CSI on a different frequency than the channel where the precoder is used. In these conditions the mean sum-rates for ZF and SLNR are reduced to about 48–90% (range of 10%- to 90%-percentile among scenarios) of the performance with ideal CSI and 64 elements, and where the actual and estimated CSI is offset by 1.3 MHz. The largest degradation is for scenarios where the user channels are least separated in angle. For MRT the range is 73–96%, and thus the ZF and SLNR precoders are the most sensitive towards frequency offset.

REFERENCES

[1] J. Zhang, Z. Zheng, Y. Zhang, J. Xi, X. Zhao, and G. Gui, "3D MIMO for 5G NR: Several observations from 32 to massive 256 antennas based on channel measurement," *IEEE Commun. Mag.*, vol. 56, no. 3, pp. 62–70, Mar. 2018.

[2] D. Gesbert, M. Kountouris, R. W. Heath, Jr., C.-B. Chae, and T. Salzer, "Shifting the MIMO paradigm," *IEEE Signal Process. Mag.*, vol. 24, no. 5, pp. 36–46, Sep. 2007.
[3] T. L. Marzetta, "Noncooperative cellular wireless with unlimited numbers of base station antennas," *IEEE Trans. Wireless Commun.*, vol. 9, no. 11, pp. 3590–3600, Nov. 2010.
[4] X. Gao, O. Edfors, F. Rusek, and F. Tufvesson, "Massive MIMO performance evaluation based on measured propagation data," *IEEE Trans. Wireless Commun.*, vol. 14, no. 7, pp. 3899–3911, Jul. 2015.
[5] J. Flordelis, F. Rusek, F. Tufvesson, E. G. Larsson, and O. Edfors, "Massive MIMO performance—TDD versus FDD: What do measurements say?" *IEEE Trans. Wireless Commun.*, vol. 17, no. 4, pp. 2247–2261, Apr. 2018.
[6] G. Liu, X. Hou, J. Jin, F. Wang, Q. Wang, Y. Hao, Y. Huang, X. Wang, X. Xiao, and A. Deng, "3-D-MIMO with massive antennas paves the way to 5G enhanced mobile broadband: From system design to field trials," *IEEE J. Sel. Areas Commun.*, vol. 35, no. 6, pp. 1222–1233, Jun. 2017.
[7] S. Zhang, P. Harris, A. Doufexi, A. Nix, and M. Beach, "Massive MIMO real-time channel measurements and theoretic TDD downlink throughput predictions," in *Proc. IEEE 27th Annu. Int. Symp. Pers., Indoor, Mobile Radio Commun. (PIMRC)*, Sep. 2016, pp. 1–6.
[8] P. Harris, W. B. Hasan, S. Malkowsky, J. Vieira, S. Zhang, M. Beach, L. Liu, E. Mellios, A. Nix, S. Armour, A. Doufexi, K. Nieman, and N. Kundargi, "Serving 22 users in real-time with a 128-antenna massive MIMO testbed," in *Proc. IEEE Int. Workshop Signal Process. Syst. (SiPS)*, Oct. 2016, pp. 266–272.
[9] P. Harris, S. Zhang, M. Beach, E. Mellios, A. Nix, S. Armour, A. Doufexi, K. Nieman, and N. Kundargi, "LOS throughput measurements in real-time with a 128-antenna massive MIMO testbed," in *Proc. IEEE Global Commun. Conf. (GLOBECOM)*, Dec. 2016, pp. 1–7.
[10] X. Wang, T. Tian, T. Kashima, X. Hou, H. Jiang, A. Benjebbour, Y. Saito, Y. Kishiyama, J. Qiu, H. Shen, and C. Tang, "Large scale experimental trial of 5G mobile communication systems—TDD massive MIMO with linear and non-linear precoding schemes," in *Proc. IEEE 27th Annu. Int. Symp. Pers., Indoor, Mobile Radio Commun. (PIMRC)*, Sep. 2016, pp. 1–5.
[11] Y. Saito, A. Benjebbour, Y. Kishiyama, X. Wang, X. Hou, H. Jiang, L. Lu, W. Liang, B. Li, L. Gu, Y. Cui, and T. Kashima, "Large scale field experimental trial of downlink TDD massive MIMO at the 4.5 GHz band," in *Proc. IEEE 85th Veh. Technol. Conf. (VTC Spring)*, Jun. 2017, pp. 1–5.
[12] J. Hoydis, C. Hoek, T. Wild, and S. ten Brink, "Channel measurements for large antenna arrays," in *Proc. Int. Symp. Wireless Commun. Syst. (ISWCS)*, Aug. 2012, pp. 811–815.
[13] À. O. Martínez, E. De Carvalho, and J. Ø. Nielsen, "Towards very large aperture massive MIMO: A measurement based study," in *Proc. IEEE Globecom Workshops (GC Wkshps)*, Dec. 2014, pp. 281–286.
[14] J. Flordelis, X. Gao, G. Dahman, F. Rusek, O. Edfors, and F. Tufvesson, "Spatial separation of closely-spaced users in measured massive multi-user MIMO channels," in *Proc. IEEE Int. Conf. Commun. (ICC)*, Jun. 2015, pp. 1441–1446.
[15] À. O. Martínez, J. Ø. Nielsen, E. De Carvalho, and P. Popovski, "An experimental study of massive MIMO properties in 5G scenarios," *IEEE Trans. Antennas Propag.*, vol. 66, no. 12, pp. 7206–7215, Dec. 2018.
[16] J. Flordelis, F. Rusek, X. Gao, G. Dahman, O. Edfors, and F. Tufvesson, "Spatial separation of closely-located users in measured massive MIMO channels," *IEEE Access*, vol. 6, pp. 40253–40266, 2018.
[17] P. Harris, W. Boukley Hasan, L. Liu, S. Malkowsky, M. Beach, S. Armour, F. Tufvesson, and O. Edfors, "Achievable rates and training overheads for a measured LOS massive MIMO channel," *IEEE Wireless Commun. Lett.*, vol. 7, no. 4, pp. 594–597, Aug. 2018.
[18] C. Shepard, J. Ding, R. E. Guerra, and L. Zhong, "Understanding real many-antenna MU-MIMO channels," in *Proc. 50th Asilomar Conf. Signals, Syst. Comput.*, Nov. 2016, pp. 461–467.
[19] J. Ø. Nielsen, W. Fan, P. C. F. Eggers, and G. F. Pedersen, "A channel sounder for massive MIMO and mmWave channels," *IEEE Commun. Mag.*, vol. 56, no. 12, pp. 67–73, Dec. 2018.
[20] *Danish Map Supply*. Accessed: Oct. 23, 2020. [Online]. Available: https://kortforsyningen.dk/indhold/english
[21] E. Björnson, M. Bengtsson, and B. Ottersten, "Optimal multiuser transmit beamforming: A difficult problem with a simple solution structure [Lecture Notes]," *IEEE Signal Process. Mag.*, vol. 31, no. 4, pp. 142–148, Jul. 2014.
[22] E. Björnson, "Optimal resource allocation in coordinated multi-cell systems," *Found. Trends Commun. Inf. Theory*, vol. 9, nos. 2–3, pp. 113–381, 2013, doi: 10.1561/0100000069.
[23] X. Chen, A. Liu, Y. Cai, V. K. N. Lau, and M.-J. Zhao, "Randomized two-timescale hybrid precoding for downlink multicell massive MIMO systems," *IEEE Trans. Signal Process.*, vol. 67, no. 16, pp. 4152–4167, Aug. 2019.
[24] C. B. Peel, B. M. Hochwald, and A. L. Swindlehurst, "A vector-perturbation technique for near-capacity multiantenna multiuser communication—Part I: Channel inversion and regularization," *IEEE Trans. Commun.*, vol. 53, no. 1, pp. 195–202, Jan. 2005.
[25] A. Müller, R. Couillet, E. Björnson, S. Wagner, and M. Debbah, "Interference-aware RZF precoding for multicell downlink systems," *IEEE Trans. Signal Process.*, vol. 63, no. 15, pp. 3959–3973, Aug. 2015.
[26] A. Ghazanfari, H. V. Cheng, E. Björnson, and E. G. Larsson, "Enhanced fairness and scalability of power control schemes in multi-cell massive MIMO," *IEEE Trans. Commun.*, vol. 68, no. 5, pp. 2878–2890, May 2020.
[27] E. Björnson, M. Bengtsson, and B. Ottersten. *MATLAB*. [Online]. Available: https://github.com/emilbjornson/optimal-beamforming
[28] *5G; NR; Physical Channels and Modulation*, document 3GPP TS 38.211 version 15.7.0 release 15, 2019. [Online]. Available: http://www.etsi.org/standards-search

JESPER ØDUM NIELSEN received the master's degree in electronics engineering and the Ph.D. degree from Aalborg University, Denmark, in 1994 and 1997, respectively. He is currently with the Department of Electronic Systems, Aalborg University, Denmark, in the antennas, propagation, and millimeter-wave systems section. His main areas of interest include experimental investigation of the mobile radio channel and the influence mobile device users have on the channel. Among other things, he has been involved in massive MIMO and mm-wave channel sounding and modeling, as well as measurements using live LTE networks. In addition, he has been working with radio performance evaluation, including over the air testing of active wireless devices.

ANDERS KARSTENSEN is currently pursuing the Ph.D. degree with the Department of Electronic Systems, Faculty of Engineering and Science, Antennas, Propagation, and Millimeter-Wave Systems Section, Aalborg University, Denmark. His main research interests include massive multiple-input and multiple-output channel modeling.

PATRICK C. F. EGGERS (Member, IEEE) was born in Stockholm, Sweden, in 1957. He received the M.Sc.E.E. and Ph.D. degrees from Aalborg University, in 1984 and 2003, respectively. From 1988 to 1989, he was with Telecom New Zealand, where he was involved in multi diffraction path-loss modeling. He is currently an Associate Professor with the Antennas, Propagation and Millimeter-Wave Systems Section, Aalborg University. He has been responsible for the planning and analysis of propagation work in domestic and EU projects, such as TSUNAMI, CELLO, and i-Rotor. He is the Initiator of the M.Sc.E.E. course at Aalborg University, specializing in wireless communication. He has over 130 publications in journals, conference proceedings, and books. He has 11 filed or granted patents. His research interests include angular propagation characteristics related to multi-antenna system operation and statistical channel modeling (e.g., ultra-reliable communication), and channel characterization in harsh environments relevant for the TETRA system or sensor-based systems with near-field disturbances. He received the Best Paper Award at the IEEE VTC Fall 2007. He has participated actively in earlier wireless communications related COST actions, starting from COST 207.

ELISABETH DE CARVALHO (Senior Member, IEEE) received the Ph.D. degree in electrical engineering from Télécom ParisTech, France, in 1999. After her Ph.D. degree, she was a Postdoctoral Fellow at Stanford University, Stanford, CA, USA, and then worked in industry in the field of DSL and wireless LAN. Since 2005, she has been with Aalborg University, where she is currently a Professor, and has led several research projects in wireless communications. She has coauthored the book "Practical Guide to MIMO Radio Channel." Her main expertise is in the field of signal processing, with the emphasis on MIMO communications. She is a member of the IEEE Signal Processing Society, Technical Committee "Signal Processing for Communications and Networking" (SPCOM), and the Vice Chair of the IEEE COMSOC Emerging Technology Initiative on Machine Learning for Communications. She is the Project Manager of the H2020 Innovative Training Network WindMill, focusing on machine learning for wireless communications.

GERHARD STEINBÖCK received the D.I. (FH) degree in telecommunications from Technikum Wien, Austria, in 1999, and the M.Sc.E. *(cum laude)* and Ph.D. degrees in wireless communications from Aalborg University, Denmark, in 2008 and 2013, respectively. From 2000 to 2006, he worked as a R&D Engineer with the Austrian Institute of Technology (AIT), Vienna, Austria, contributing among other things in the hard- and software development of a real-time radio channel emulator. After continuing as a Postdoctoral Researcher at Aalborg University, he joined Huawei Technologies Sweden AB, in 2016. His research interests include the area of wireless communications, systems simulation, radio channel modeling, radio channel estimation and sounding, and radio geolocation techniques.

MARTIN ALM received the M.Sc. degree in electrical engineering from the Chalmers University of Technology, Sweden, in 1995. Since then, he has worked at Ericsson and Huawei, with antennas, propagation, and signal processing in radar and wireless communication contexts. His main research interest includes massive MIMO system design.